HNPS Advances in Nuclear Physics

Vol 2 (1991)

HNPS1991

GENERAL CHARACTERISTICS OF INTERMEDIATE MASS FRAGMENT INCLUSIVE CROSS SECTIONS IN 20Ne INDUCED INTERACTIONS

N. H. Papadakis, - et al.

doi: 10.12681/hnps.2841

GENERAL CHARACTERISTICS OF INTERMEDIATE MASS FRAGMENT INCLUSIVE CROSS SECTIONS IN ^{20}Ne INDUCED INTERACTIONS

N.H.PAPADAKIS[1], N.P.VODINAS[1*], Y.CASSAGNOU[2], R.DAYRAS[2], R.FONTE[3], G.IMME[3], R.LEGRAIN[2], A.D.PANAGIOTOU[1], E.C.POLLACCO[2], G.RACITI[3], L.RODRIGUEZ[2], F.SAINT-LAURENT[4], M.G.SAINT- LAURENT[4], and N.SAUNIER[2]

[1] Physics Department, Nuclear and Particle Physics Division, University of Athens, Panepistimiopolis, GR-15771 Athens, Greece

[2] Departement de Physique Nucleaire - SEPN, C.E.N. Saclay, 91191 Gif-sur-Yvette Cedex, France

[3] INFN-LNS and Physics Department, University of Catania, 57 Corso Italia, Catania I-95129 , Italy

[4] GANIL, B.P.5027, F-14021 Caen Cedex, France

Abstract

Inclusive integrated cross sections of intermediate mass fragments have been measured in ^{20}Ne induced reactions on silver and gold targets at 20, 30, 40, 50 and 60 MeV/nucleon incident energies. Whereas the production yields remain approximately constant for the Ne+Ag system, for incident energies greater than 30 MeV/nucleon, they increase by a factor of 3.5 for the Ne+Au system over the full energy range studied.

*Presented by N.P.Vodinas

1 Introduction

When an energetic strongly interacting projectile collides with a heavy target nucleus, complex nuclei (fragments) with $A \geq 6$ are produced in a process called nuclear fragmentation [1]. Especially fragments with $6 \leq A \leq 40$ (e.g. fragments heavier than a-particles, but lighter than fission fragments) are attributed to a process termed intermediate mass fragment (IMF) emission [2].

Up to now there is no consensus concerning the origin of IMF and their emission has been the subject of many theoretical and experimental investigations. The current models can be classified in two main classes: "binary" (direct binary, statistical binary, sequential binary), typical of low incident energy regime and "multi-fragmentation" (statistical multi-fragmentation, dynamical multi-fragmentation), expected for higher energies. Depending also on the degree of thermalization, the fragmentation models may be divided in those of thermal equilibrium and those of cold nonequilibrium breakup [2,3,4,5].

Recently heavy ion beams in the intermediate energy range (10-100 MeV/nucleon) have been available for the experimentalists. This energy range is fascinating in several aspects: i) This is obviously a region where the nature of nuclear collisions is expected to change from low energy to high energy behavior. However, how rapidly this transition occurs is still an open question. ii) Interaction times become comparable to or even shorter than relaxation times of the intrinsic degrees of freedom. Thus one expects non-equilibrium phenomena to increase in importance. iii) The velocity of the projectile becomes comparable or greater than characteristic velocities in the nucleus such as the sound velocity ($\sim$0.15c) [6] and the Fermi velocity ($\sim$0.3c). By passing those different thresholds, qualitative new mechanisms may be expected to occur. It is therefore very interesting to study nuclear fragmentation phenomena in the intermediate energy region.

In the case of nucleus-nucleus collisions IMF are the products of the decay of various "sources", such as "sources" related to the projectile or to the target or to the compound system or "sources" with no obvious

relationship with either target or projectile [7]. These "sources" have different contribution to the IMF production depending on the angular range, energy and mass of the emitted fragments and their respective contribution vary with incident energy [8,9,10].

In studying nuclear fragmentation processes, it is customary to try to separate the contributions of the various "sources" by appropriate "cuts" in the experimental data (in the angular range, in the velocity of the fragments, etc), or by model-dependent fits, or by exclusive measurements. In a different way, the systematic evolution of the fragment yield with bombarding energy or with projectile-target combination and irrespective of the emitting "source" could reveal general features which are dependent on the mass of the system, the total available energy for excitation or the linear momentum transfer.

In this contribution we present and investigate, in a systematic and consistent way, inclusive angle and energy integrated cross sections of Z-separated IMFs for ^{20}Ne induced reactions on gold and silver targets, in a large energy range between 20 and 60 MeV/nucleon.

2 Experimental Techniques

The experiments were performed at the GANIL National Laboratory. The target and detector systems were installed inside the 3-meter long by 3-meter diameter scattering chamber called NAUTILUS. Cryogenic pumping maintained a hydrocarbon-free vacuum of 10^{-7} Torr. The ^{20}Ne beam with 20, 30, 40, 50, 60 MeV/nucleon incident energy, bombarded self-supporting targets of natural Ag and Au. At 50 and 60 MeV/nucleon incident energies 5.2 mg/cm^2 Ag and 10 mg/cm^{2}Au thick targets were used, while at the other energies thinner Ag and Au targets of 0.36 and 1.33 mg/cm^2, respectively, were bombarded. Their thicknesses were measured via the energy loss of alpha particles from a ^{228}Th source. The target angle was chosen to give an overall optimum energy resolution.

The types and characteristics of the detectors are presented in Table 1. As detector system we have used four telescopes (C, D, E, F) each con-

Table 1: Types and Characteristics of Detectors

DETECTOR	*TYPE*	*THICKNESS*	*SURFACE* (mm^2)
C_1	ΔE(I.Ch)	7.2 cm	
C_2	ΔE(Si)	311 μm	300
C_3	E(SiLi)	4600 μm	300
D_1	ΔE(I.Ch)	7.2 cm	
D_2	ΔE(Si)	318 μm	300
D_3	E(SiLi)	4100 μm	300
E_1	ΔE(I.Ch)	5 cm	
E_2	E(Si)	500 μm	300
F_1	ΔE(I.Ch)	5 cm	
F_2	E(Si)	500 μm	300

sisted of a ionization chamber (ΔE_1) associated with a single (E) or double (ΔE_2 + E) silicon counter. These telescopes, devoted to the detection of IMF, were mounted on remotely controlled arms, independently rotating in the horizontal plane. The rotation angles were set with an accuracy of $\pm$ 0.01 deg. In order to identify charges in an extended energy range, transverse field ionization chambers were used as ΔE_1. The larger C and D chambers, with a useful length of 7.2 cm, were filled with a mixture of argon-methane (90%-10%). They were operated at a pressure of 141 Torr during the runs at 20, 30 and 40 MeV/nucleon and at 167 Torr during the 50 and 60 MeV/nucleon runs. They were positioned at 117.4 cm from the target, subtending a solid angle of 0.17 msr. The two small ionization chambers E and F, with a useful length of 5 cm, used the same gas mixture at 61 Torr at all energies. They were located at 24.4 cm from the target and subtended 0.63 msr solid angle. Having such a larger solid angle, they were appropriate for measurements of small fragment yields at the backward angles.

The fast signals from the second detector in each telescope were used in the triggering logic for the CAMAC driven data acquisition system. The raw data were recorded event-by-event on magnetic tape.

The energy calibration of the silicon detectors was achieved through a precision pulser calibrated against a three alpha-source (^{241}Am, ^{244}Cm and

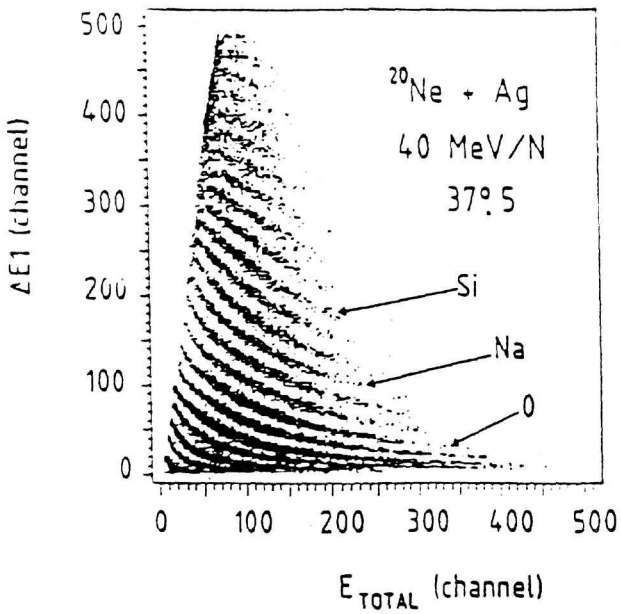

Figure 1: Elemental two-dimensional ΔE_1-E_{TOTAL} plot for the system ^{20}Ne+Ag at 40 MeV/nucleon incident energy.

^{239}Pu). To calibrate the ionisation chambers, the energy loss of the alpha particles from the source were determined by measuring residual energies in the silicon detectors with and without gas in the chambers.

3 Experimental Data and Discussion

The fragments were detected over the angular range of $15.5 \leq \theta_{lab} \leq 127.5$ deg. at 20, 30, 40 MeV/nucleon and $22.7 \leq \theta_{lab} \leq 113.3$ deg. at 50 and 60 MeV/nucleon incident energies. The event-by-event data were analyzed off-line. Element identification was obtained from the plots of ΔE_1 versus total energy, $E_{TOTAL}=\Delta E_1+(\Delta E_2)+E$. Typical elemental two-dimensional ΔE_1-E_{TOTAL} plots, obtained for the ^{20}Ne+Ag system at 40 MeV/nucleon is shown in Figure 1. The energy spectra for each fragment type were obtained by setting windows on the ΔE_1-E_{TOTAL} plots. Integrating the energy spectra over the particle energy we obtained the differential cross sections, $d\sigma(\theta)/d\Omega$, for each element. Statistical errors and a 30% er-

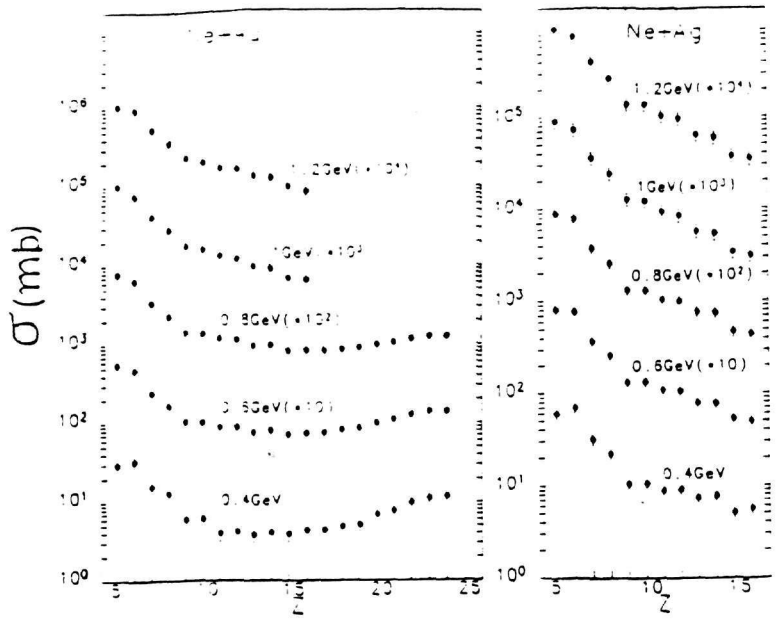

Figure 2: Charge distributions for Ne+Ag and Ne+Au systems at 20, 30, 40, 50, and 60 MeV/nucleon beam energy. The cross sections were obtained by integrating the angular distributions in the angular range $22.5 \leq \theta_{lab} \leq 112.5$ deg.

ror in the normalization constant arising from the target thickness and integrated beam charge uncertainties, were taken into account in the evaluation of the total error in the differential cross section.

The integrated cross section for each fragment was obtained by integrating the angular distributions using the equation:

$$\sigma = 2\pi \int_{\theta_{min}}^{\theta_{max}} (d\sigma/d\Omega) \sin\theta d\theta \qquad (1)$$

The integration of the angular distributions was carried over the angular range θ_{min}=22.5deg. to θ_{max}=112.5deg., in order to have a common range. By taking into account the uncertainty of each point in the angular distribution, integrated cross sections have an estimated uncertainty of less than 20%.

Charge distributions (i.e. cross sections as a function of charge of the fragments) are shown in Figure 2 as a function of the beam energy.

For the Ne+Ag system a monotonic decrease of the fragment yield with the atomic number is observed at all incident energies. For the Ne+Au system there are considerable differences with respect to the energy, since an energy-dependent extension of the fission tail is present which causes a U-shaped charge distribution. As a result, the monotonic decrease of the fragment yield is observed to stop approximately at Z=11, 13 and 15 for incident energies of 20, 30 and 40 MeV/nucleon, respectively. For the higher energies of 50 and 60 MeV/nucleon, there is an indication that the monotonic decrease continues beyond Z=15. Such a difference between Ag and Au targets has also been observed for ^{12}C and ^{32}S induced reactions [11,12].

Figure 3 (upper case) shows the fragment yields for typical Z-values as a function of the incident energy for both systems. For Ne+Au, the inclusive cross section for Z=6 and Z=11 fragments increases almost exponentially with bombarding energy. However, the rise of the Z=11 yield is more pronounced compared to that for Z=6, indicating that apparently the production of heavy fragments ($Z > Z_{beam}$) increases more rapidly than the one of light fragments ($Z < Z_{beam}$) with increasing bombarding energy. The reason could be that at low bombarding energy (20 MeV/nucleon) projectile fragmentation contributes to the yield of the light fragments at the more forward angles due to an increase of the grazing angle. In contrast, for Ne+Ag the fragment yields for Z=6, 11 and 16 are nearly independent of incident energy, indicating that the main contribution to the fragment yield has the same origin for $Z < Z_{beam}$ and $Z > Z_{beam}$.

The dependence of the inclusive fragment production cross section upon incident energy is shown in Figure 3 (lower case) for the two systems. In order to make meaningful comparisons for the two systems the production cross sections for elements with $5 \leq Z \leq 11$ were considered in the case of the Ne+Au reaction, whereas elements with $5 \leq Z \leq 16$ and with $5 \leq Z \leq 11$ were taken into account in the case of the Ne+Ag reaction. A noteworthy difference between the two reactions is observed. For the Ne+Au the sum of the non-fission cross sections increases as a function of incident energy, in agreement with data at higher energies [13]. In contrast, for Ne+Ag, in the same energy domain, the sum of the cross sections for fragments with $5 \leq Z \leq 16$ ($5 \leq Z \leq 11$) increases between 20 and 30 MeV/nucleon incident

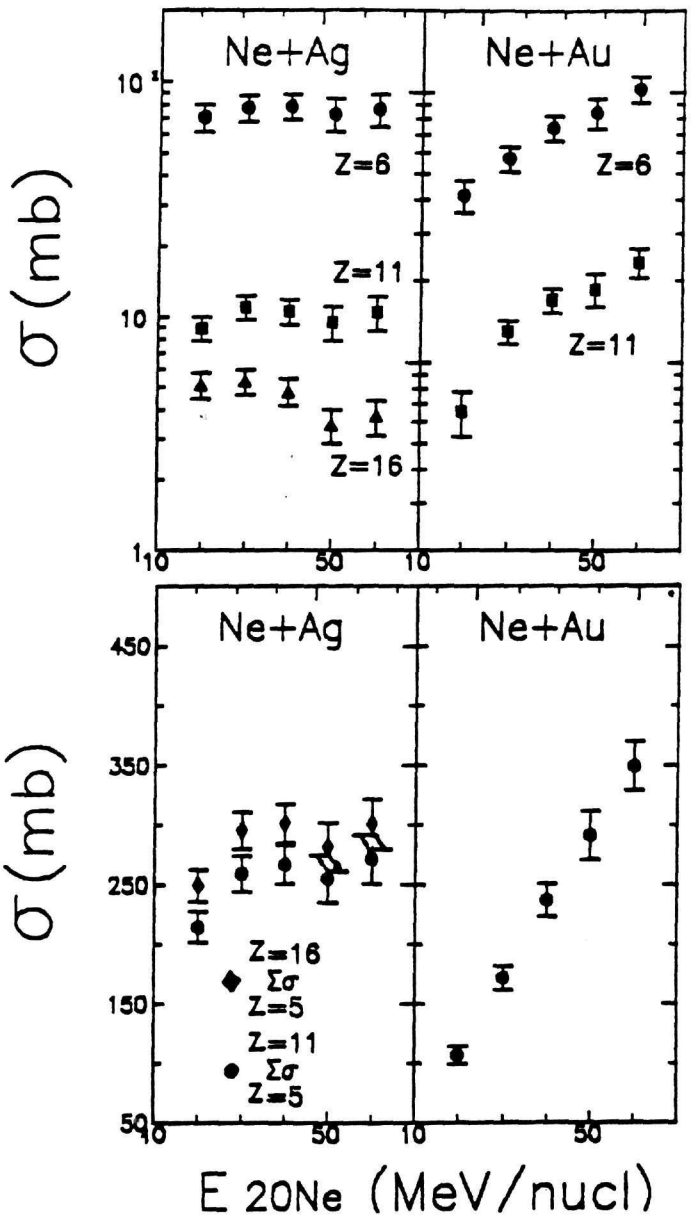

Figure 3: Integrated cross sections for given Z (upper case) and summed cross sections (lower case) as a function of incident energy for the Ne+Ag and Ne+Au systems. The cross sections were obtained by integrating the angular distributions in the angular range $22.5 \leq \theta_{lab} \leq 112.5$ deg.

energies and then, for greater beam energies, remains roughly constant. We note in Figure 3 (lower case) that at energies below 50 MeV/nucleon the cross section in the charge range $5 \leq Z \leq 11$ for silver is greater than for gold and becomes comparable at 50 MeV/nucleon.

Such a difference in the evolution of the fragment cross section with incident energy can be associated with the fact that the available energy per nucleon is always higher for Ne+Ag than for Ne+Au. Thus for Ne+Ag system, the fragmentation regime may be established at the lowest bombarding energy, whereas for Ne+Au it sets in, in the energy range considered.

A recent publication [10] has studied IMF production in ^{14}N induced reactions on Ag and Au at 20-50 MeV/nucleon incident energies. In contrast to our data, the IMF production yield is slightly higher for the gold target than for the silver target. The difference might be due in part to the fact that we have considered only fragments with $Z \geq 5$ whereas they have considered fragments with $Z \geq 3$, the lighter fragments being more abundantly produced with gold target.

4 Summary

In summary, we have presented data from ^{20}Ne induced reactions on Ag and Au targets which represent inclusive measurements of IMF integrated (in the angular range $22.5 \leq \theta_{lab} \leq 112.5$ deg.) cross sections over a large range of incident energies in the intermediate energy domain. They present a marked target effect. Charge distributions decrease monotonically for Ag target at all incident energies whereas for Au target the fission component causes an energy U-shaped behavior, at lower incident energies. With increasing energy, the Ag target shows a saturation effect while for Au the cross section increases monotonically. These results suggest that in the case of Ag, the fragmentation regime is reached well within the energy range studied. On the other hand, in the case of Au, the fragmentation process still develops between 20 and 60 MeV/nucleon, in connection with a lower available energy per nucleon.

References

[1] A. Bujak et al., Phys. Rev. C32 (1985) 620
[2] W. G. Lynch, Ann. Rev. Nucl. Sci. 37 (1987) 493
[3] J. Huefner, Phys. Rep. 125, No 4 (1985) 129
[4] L. G. Moretto et al., preprint LBL-24558 (1987)
[5] J. Aichelin et al., Phys. Rev. C30 (1984) 107
[6] J. P. Blaizot, Phys. Rep. 64 (1980) 171
[7] B. Borderie, Journal de Physique 47 Coll. C4 (1986) 259
[8] R. Trockel, PhD Thesis, University of Heidelberg (1987), GSI-87-17
[9] N.H. Papadakis, PhD Thesis, University of Athens (1988), N.H. Papadakis et al., " Inclusive Production of Intermediate Mass Fragments in ^{20}Ne+Ag, Au Interactions at 20-60 MeV/nucleon ", Contribution to this Symposium.
[10] D.E.Fields et al., Phys. Lett. B220 (1989) 356
[11] C. Chitwood et al., Phys. Lett. B131 (1987) 289
[12] A. Lleres et al., Phys. Lett. B187 (1987) 336
[13] A.I.Warwick et al., Phys. Rev. C27 (1983) 1083